Thin Solid Films xxx (2014) xxx–xxx

Contents lists available at ScienceDirect

Thin Solid Films

journal homepage: www.elsevier.com/locate/tsf

Composition variations in $Cu_2ZnSnSe_4$ thin films analyzed by X-ray diffraction, energy dispersive X-ray spectroscopy, particle induced X-ray emission, photoluminescence, and Raman spectroscopy

Dahyun Nam [a], A.S. Opanasyuk [b], P.V. Koval [b], A.G. Ponomarev [b], Ah Reum Jeong [c], Gee Yeong Kim [c], William Jo [c], Hyeonsik Cheong [a,*]

[a] Department of Physics, Sogang University, Seoul 121-742, Republic of Korea
[b] Department of Electronics and Computer Technology, Sumy State University, Sumy UA-40007, Ukraine
[c] Department of Physics, Ewha Womans University, Seoul 120-750, Republic of Korea

ARTICLE INFO

Article history:
Received 10 August 2013
Received in revised form 24 March 2014
Accepted 26 March 2014
Available online xxxx

Keywords:
Copper–zinc–tin selenide
Thin films
X-ray diffraction
Energy dispersive X-ray spectroscopy
Raman spectroscopy
Confocal microscopy
Particle induced X-ray emission
Photoluminescence

ABSTRACT

Compositional and structural studies of $Cu_2ZnSnSe_4$ (CZTSe) thin films were carried out by X-ray diffraction, energy dispersive X-ray spectroscopy (EDS), particle induced X-ray emission (PIXE), photoluminescence, and Raman spectroscopy. CZTSe thin films with different compositions were deposited on sodalime glass by co-evaporation. The composition of the films measured by two different methods, EDS and PIXE, showed significant differences. Generally, the Zn/Sn ratio measured by EDS is larger than that measured by PIXE. Both the micro-PIXE and the micro-Raman imaging results indicated the compositional and structural inhomogeneity of the sample.

1. Introduction

$Cu_2ZnSnSe_4$ (CZTSe) thin films have attracted much attention recently due to their application as an absorber layer of thin film solar cells. Because CZTSe does not contain scarce materials such as indium and gallium, it is thought to be more suitable for mass production. The band gap of CZTSe has been determined to be approximately 1.0 eV [1,2]. Its crystal structure is considered to be kesterite based on neutron scattering measurements [3], but with only 3–4 meV/atom difference from the stannite structure [4,5]. So far, most studies on CZTSe thin films have been focused on optimizing the solar cell performances, but the material properties at the microscopic scales have not been investigated thoroughly. Various methods have been used to grow CZTSe including both non-vacuum and vacuum methods. So far the highest efficiency of 9.2% has been achieved by the sputtering method [6]. Experimentally, the composition of Cu/(Zn + Sn) ~ 0.8 and Zn/Sn ~ 1.2 has given the highest solar cell efficiencies [7–9]. Chen et al. theoretically explained that defect clusters such as $Cu_{Zn} + Sn_{Zn}$ and $2Cu_{Zn} + Sn_{Zn}$ can form even in stoichiometric samples and that Zn-rich and Cu, Sn-poor conditions are required to prevent their formation and increase the efficiency [10,11]. However, formation of secondary phases such as ZnSe, Cu_2SnSe_3 (CTSe), and CuSe is difficult to avoid under this nonstoichiometric condition. Also, such secondary phases may be distributed inhomogeneously throughout the film [12,13]. Therefore, a precise knowledge of the composition in microscopic scale is essential in fine-tuning the growth conditions for the best solar cell performances. The composition values in most studies are obtained from energy-dispersive X-ray-spectroscopy (EDS) or X-ray fluorescence measurements. However, these techniques are not sensitive enough to determine the composition at the $\mu g \cdot g^{-1}$ level [14]. Proton-induced X-ray emission (PIXE), on the other hand, uses a proton beam of mega-electron-volt energy which generates many orders of magnitude less bremsstrahlung radiation than kilo-electron-volt electron beam used in EDS, giving PIXE an analytical sensitivity several orders better than that of EDS [15]. Furthermore, the proton beam can be focused so that local composition in micro-meter scale can be probed. Therefore, the PIXE technique gives more accurate results with high sensitivity and spatial resolution and has been

* Corresponding author. Tel./fax: +82 2 717 8434.
E-mail address: hcheong@sogang.ac.kr (H. Cheong).

http://dx.doi.org/10.1016/j.tsf.2014.03.079
0040-6090/

used in various elemental analysis applications [14,15]. In this work, we compared PIXE measurements with EDS results from CZTSe samples and found that the PIXE results are more consistent with photoluminescence (PL) and Raman spectroscopy measurements.

2. Experimental details

2.1. Samples

Four different samples were deposited on Mo-coated sodalime glass using an electron-beam evaporation system. We used 99.999% Cu, Zn, Sn and Se raw materials from CERAC (U.S.A.). In order to deposit the films homogeneously, the substrate was rotated during the deposition process. Also, the temperature of the substrate was kept at 400 °C in order to minimize Sn loss and formation of secondary phases [16]. We controlled the deposition rate and the deposition time of each sources to make four different samples with different compositions. The details of the e-beam evaporation system and the deposition process are described in Ref. [17]. The thicknesses of the samples vary from 1.25 to 2.25 μm as obtained by secondary-ion mass spectroscopy depth profiling measurements.

2.2. Measurements

Structural investigations were carried out using an X-ray diffractometer DRON 4-07 (Ni-filtered Kα radiation of a Cu anode). The spectra were registered in the angle range (2θ) of 10° to 90°, where 2θ is the Bragg angle. The phase analysis was carried out by comparing interplane distances and specific intensities of the diffraction patterns from the samples with the data from JCPDS (CZTSe 01-070-8930). The proton microprobe with the PIXE technique (micro-PIXE) [18] was used to obtain elemental concentrations in the region of interest and to map element distributions. The energy of the proton beam was 1.5 MeV, the probe dimension about 4 μm, and the collected charge ~5×10^{-10} C/pixel. The scan region was 50×50 pixels^2, with a scanning step of 4 μm. Elemental concentrations were also measured with an EDS system, attached to a scanning electron microscope with an acceleration voltage of 15 kV. Calibration was done by using Co as a standard element. Raman spectroscopy measurements were carried out in ambient conditions with three lasers as excitation sources: the 632.8 nm-line of a He–Ne laser, the 514.5 nm-line of an Ar^+ laser, and the 441.6 nm-line of a He–Cd laser. A laser beam with a power of ~20 mW was focused to a line of ~5 mm × 50 μm in a quasi-backscattering configuration. Jobin-Yvon TRIAX 320 (632.8 nm laser) and TRIAX 550 (514.5 and 441.6 nm lasers) spectrometers (1200 grooves/mm, blazed at 500 nm) were used to disperse the signals. The slit width was fixed at 0.1 mm and a pair of RazorEdge ultrasteep long-pass edge filters (Semrock) was used to eliminate the laser signals. The signals were detected with a liquid-nitrogen-cooled or thermoelectrically-cooled back-illuminated charge-coupled-device detector array. Micro-Raman measurements were performed by focusing the laser beam with a 50× microscope objective (0.8 N.A.) to a spot of ~1 μm in diameter. Micro-Raman imaging measurements were carried out by using the 514.5-nm laser with a power of 1 mW. Low temperature PL measurements were carried out in a liquid-helium closed-cycle refrigerator system at 8 K. A 514.5-nm laser with a power of 2 mW was used as the excitation source. The laser beam was focused to a sample by using a spherical lens to a ~50 μm diameter spot. The luminescence signal was dispersed and detected with a TRIAX 320 spectrometer with a grating of 600 grooves/mm, blazed at 1000 nm, and a thermoelectrically cooled InGaAs photodiode, respectively. The second order signal of the laser line was eliminated by using a long-pass color filter (RG 830), transparent to wavelengths of >830 nm.

3. Results and discussion

3.1. X-ray diffraction (XRD)

Fig. 1 shows the XRD results of the four samples. All samples show strong (112), (204), and (312) peaks which are usually assigned to kesterite CZTSe [1,19,20]. There are several weaker peaks also corresponding to kesterite CZTSe. This result indicates that the samples are polycrystalline having preferred directions, as others have already discovered. The lattice constants a and c of the CZTSe were estimated from the XRD data, and the results are listed in Table 1. The lattice constants of the samples are almost the same; $a = 0.5664$–0.5687 nm and $c = 1.1347$–1.1378 nm. The values are close to the reported ones [19,20]. However, the major peaks overlap with peaks from possible secondary phases such as ZnSe and Cu_2SnSe_3. Therefore, the XRD data alone is not sufficient to identify the thin films as kesterite CZTSe.

3.2. EDS and PIXE

For the compositional analysis, we carried out EDS and PIXE measurements, and the results are shown in Fig. 2 and Table 2. Fig. 2 shows typical PIXE spectra of the samples. The peak position and intensity give information about the identity and the amount of atoms, respectively. The measured concentrations are quite different between EDS and PIXE. EDS consistently underestimates the Sn concentration, which is similar to previous comparison of EDS and PIXE for other kinds of materials [15]. The discrepancy for other elements does not show any clear tendency. Underestimation of the Sn concentration would lead to overestimation of the Zn/Sn ratio, as shown in Table 2. For example, one would expect, based on the EDS results, that samples A, B, and C would have the ZnSe secondary phase. However, as we will see in the next section, there is no indication of the ZnSe secondary phase in the Raman spectroscopy results in samples A and C. Therefore, we conclude that the Zn/Sn ratio measured by EDS should be examined carefully by comparing with other measurements.

3.3. Raman spectroscopy

In order to investigate the crystallinity of CZTSe and the existence of secondary phases, we measured the Raman spectra of the samples using three different laser wavelengths: 514.5 nm [green laser, Fig. 3(a)], 632.8 nm [red laser, Fig. 3(b)], and 441.6 nm [blue laser, Fig. 3(c)]. The spectra in Fig. 3(a) and (b) are normalized to the main CZTSe peak at 195 cm^{-1}. The spectra taken with the green laser [Fig. 3(a)] show CZTSe-related major peaks. The Raman spectrum from sample A is a

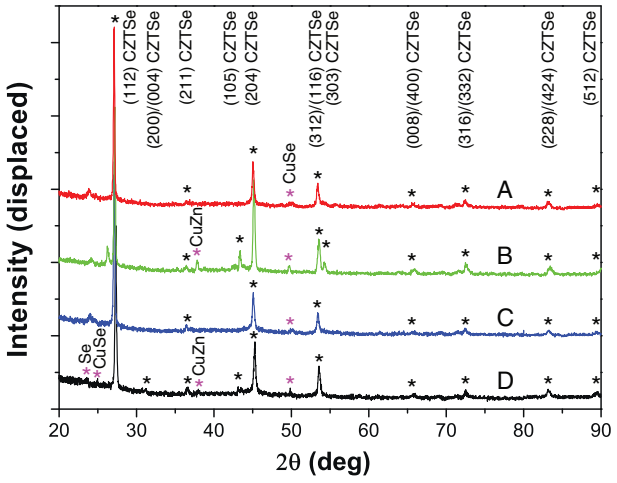

Fig. 1. XRD results. All samples show strong CZTSe phase peaks at (112), (204), and (312).

Please cite this article as: D. Nam, et al., Composition variations in $Cu_2ZnSnSe_4$ thin films analyzed by X-ray diffraction, energy dispersive X-ray spectroscopy, particle induced ..., Thin Solid Films (2014), http://dx.doi.org/10.1016/j.tsf.2014.03.079

Table 1
Lattice constants of the samples measured by XRD.

Samples	Lattice constants (XRD)		
	a (nm)	*c* (nm)	*c*/2*a*
A	0.5674	1.1347	1.000
B	0.5683	1.1378	1.001
C	0.5687	1.1354	0.999
D	0.5664	1.1348	1.002

typical Raman spectrum of CZTSe, with two distinct CZTSe peaks appearing at 172 and 195 cm^{-1}. There are two smaller peaks at 231 and 244 cm^{-1} which are also CZTSe related [21,22]. Samples B, C, and D, on the other hand, exhibit only one strong peak at 200 cm^{-1} with smaller peaks at 231 and 244 cm^{-1}. The 172 cm^{-1} peak is not resolved for these samples. These results indicate that sample A has the best crystallinity. We used the red and blue lasers to probe the existence of CTSe and ZnSe secondary phases, respectively. Because the band gap energy of CTSe is 0.84 eV [23], the red laser (1.62 eV) is more sensitive to it than the green laser (2.41 eV). Since the band gap energy of ZnSe is 2.82 eV [24], the blue laser (2.81 eV) is in resonance with the band gap, making it particularly sensitive to the existence of ZnSe [25,26].

In the Raman spectra taken with the red laser [Fig. 3(b)], samples A and D show a relatively sharp peak at 231 cm^{-1} which can be assigned to CTSe and/or CZTSe [21]. If this peak appears stronger in the spectra taken with the red laser relative to the CZTSe main peaks, one may conclude that at least part of the peak is due to CTSe because the CZTSe contribution should have the same excitation wavelength dependence as the CZTSe main peak. If we compare Fig. 3(b) with Fig. 3(a), only sample D shows a clear enhancement of this peak for the red laser excitation. Therefore, we conclude that sample D has the largest amount of the CTSe secondary phase. We should note that the main CTSe mode is supposed to appear near 180 cm^{-1}, which is between the main CZTSe peaks at 172 and 195 cm^{-1}. The asymmetry seen in the main CZTSe peak may also indicate the existence of the CTSe secondary phases. Sample D shows the largest asymmetry of the main peak, whereas samples B and C also show some degree of asymmetry. Based on these analyses, we conclude that sample D has the largest amount of CTSe and sample A has the least.

In the Raman spectra taken with the blue laser, there is only a weak broad peak in the frequency range where the ZnSe peak would normally be observed in all 4 samples, which indicates that there is not much ZnSe in these CZTSe films, at least not near the top surface of the samples. However, since sample B is significantly Zn-rich even from the PIXE analysis, one should expect at least some ZnSe formation in this sample. There has been a report that ZnSe is likely to form at the bottom close to the $MoSe_2$ layer [27]. We measured the bottom side of the films exposed by breaking the samples and found a strong ZnSe Raman signal only from sample B (not shown). These results are consistent with the

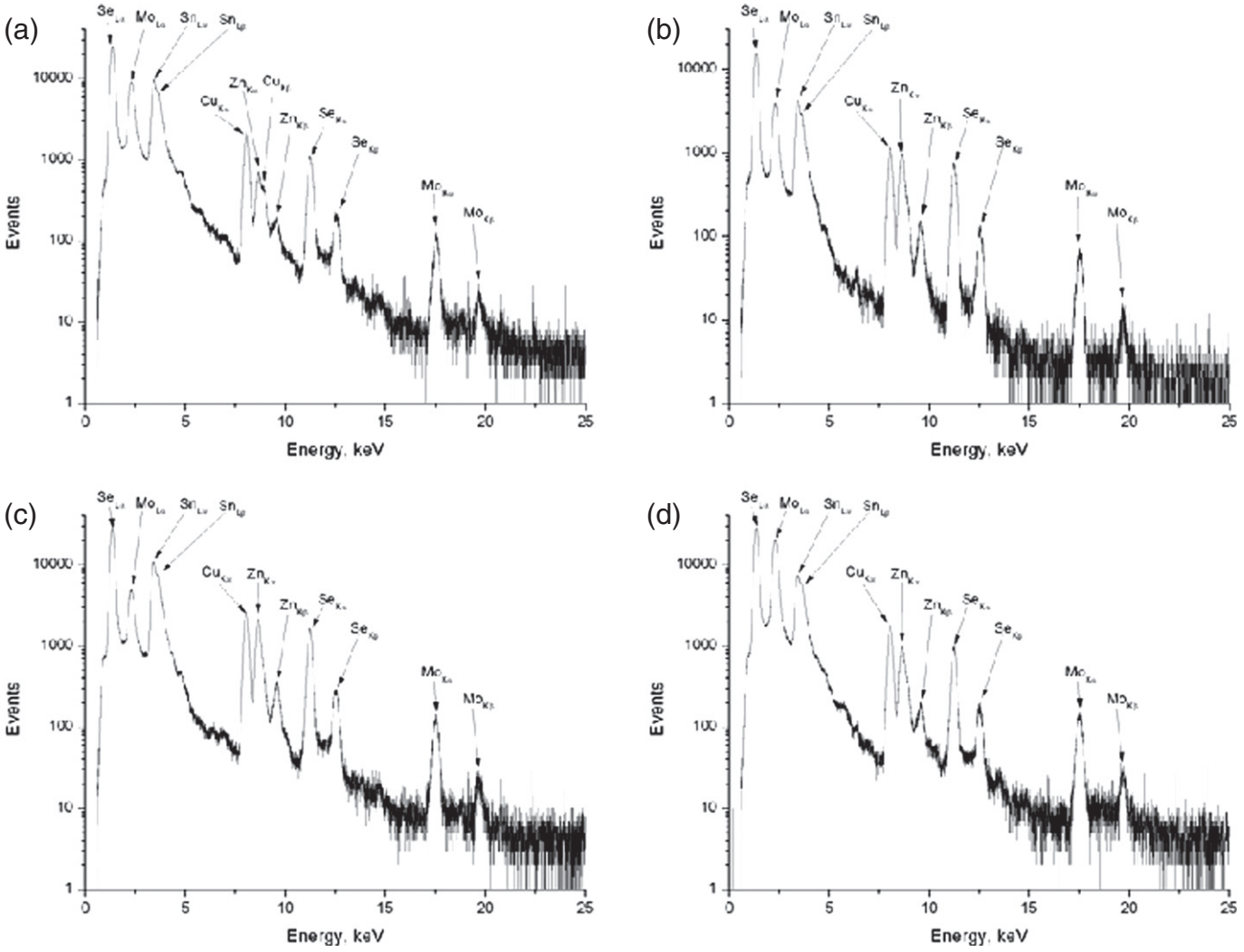

Fig. 2. Representative PIXE spectra of sample (a) A, (b) B, (c) C, and (d) D. Elements corresponding to the peaks are labeled in the figure.

Please cite this article as: D. Nam, et al., Composition variations in $Cu_2ZnSnSe_4$ thin films analyzed by X-ray diffraction, energy dispersive X-ray spectroscopy, particle induced ..., Thin Solid Films (2014), http://dx.doi.org/10.1016/j.tsf.2014.03.079

Table 2
The compositions (in at.%) of the samples measured by EDS and PIXE.

Samples	Cu	Zn	Sn	Se	Cu/Zn + Sn	Zn/Sn
	EDS[a]				Ratio	
A	29.5	13.2	10.8	46.5	1.23	1.23
B	15.7	20.8	12.3	51.2	0.474	1.69
C	22.0	14.9	12.4	50.7	0.805	1.20
D	22.4	9.03	17.6	50.9	0.842	0.513
	PIXE				Ratio	
A	18.03 ± 0.06	17.70 ± 0.09	16.36 ± 0.03	47.91 ± 0.05	0.527	1.08
B	16.81 ± 0.08	17.57 ± 0.11	13.11 ± 0.04	52.52 ± 0.07	0.547	1.33
C	19.45 ± 0.08	12.41 ± 0.10	13.91 ± 0.04	54.24 ± 0.06	0.739	0.894
D	22.11 ± 0.08	7.440 ± 0.089	18.79 ± 0.04	51.66 ± 0.06	0.840	0.406

[a] The error bars of the EDS data are approximately 10% of the measured values.

PIXE data in that only sample B is significantly Zn-rich, whereas EDS results indicate that all but sample D are Zn-rich.

3.4. Low temperature PL

Only samples A and B exhibited measurable photoluminescence. Since the PL signal is greatly reduced by the presence of defects and imperfections, it may be used as an indicator of the sample quality. Fig. 4 shows the normalized PL of the two samples. Sample A has a PL peak at around 0.77 eV and B at around 0.72 eV. Since the band gap energy of CZTSe is ~1 eV, none of these signals are due to band-to-band or shallow impurity transitions in CZTSe. These could be either from deep defect states of CZTSe or low band gap secondary phases such as CTSe, since the band gap of CTSe is 0.84 eV. Although the Raman analysis is not very conclusive about the existence of CTSe, the PL results indicate that these samples do have some CTSe phases in them. We should note that although sample D has the largest amount of CTSe, its PL is suppressed due to the poor overall crystal quality.

3.5. Micro-PIXE and micro-Raman spectroscopy

Among the four samples, sample A has the best crystallinity according to the Raman results. Therefore, we carried out micro-PIXE and micro-Raman imaging in order to check the compositional homogeneity and the crystallinity of sample A. Fig. 5(a) is a micro-PIXE image of the atomic distribution in sample A in an area of 200 × 200 μm^2 measured with a scanning step of 4 μm. In this figure the scale bars indicate the X-ray counts in each pixel or intensity which is proportional to the element concentration. It is seen that the spatial variation of the atomic compositions is quite significant. There are points where the local composition of an element is much larger (red points) or much smaller (blue points) than the surrounding areas. Similar result is shown in the micro-Raman image of the A_1 mode intensity shown in Fig. 5(b). This image was taken from sample A and the scale and the step size are the same as the micro-PIXE images, but the position is not necessarily the same as the area used in the micro-PIXE measurements. It is practically impossible to align the samples to the same positions in the two measurement systems. The Raman images were taken at several locations of the sample and showed the same pattern of lateral intensity variations. The fact that the lateral variations in the Raman peak intensity have the same overall pattern as that found in the PIXE composition maps implies that the local Raman intensity is strongly affected by the local composition of the CZTSe thin film rather than by the local crystallinity. One can conclude that either micro-PIXE or micro-Raman imaging may be used to investigate the composition inhomogeneity.

4. Conclusion

We carried out XRD, EDS, PIXE, PL and Raman spectroscopy on four CZTSe thin films with various compositions. We have found that the EDS measurements tend to underestimate the Sn composition in comparison to the PIXE measurements. The PL and Raman data showed that all samples have CZTSe phase with varying amounts of CTSe. The ZnSe secondary phase was detected on the bottom side of the most Zn-rich sample. We also found that the local composition variations observed

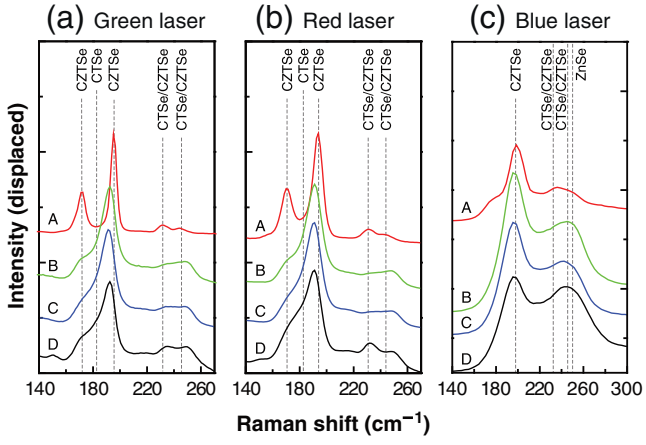

Fig. 3. Raman results of sample A–D with (a) green, (b) red and (c) blue lasers as the excitation sources. Positions of the CZTSe, CTSe, and ZnSe related peaks are indicated.

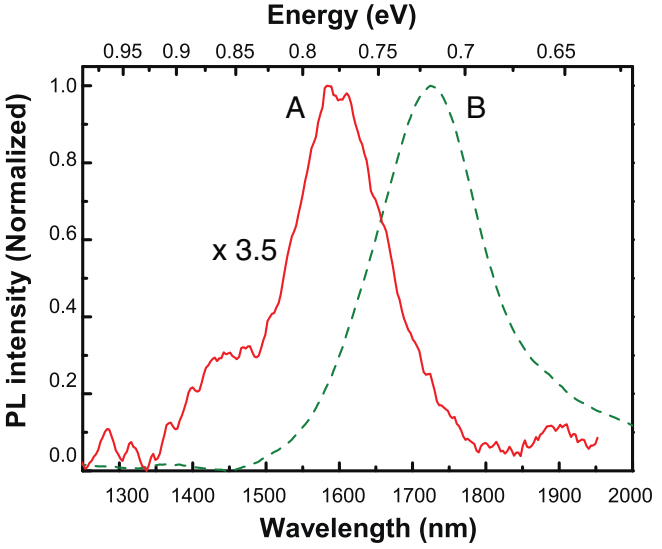

Fig. 4. Normalized PL of samples A and B at 8 K. The green laser was used as the excitation source.

Please cite this article as: D. Nam, et al., Composition variations in $Cu_2ZnSnSe_4$ thin films analyzed by X-ray diffraction, energy dispersive X-ray spectroscopy, particle induced ..., Thin Solid Films (2014), http://dx.doi.org/10.1016/j.tsf.2014.03.079

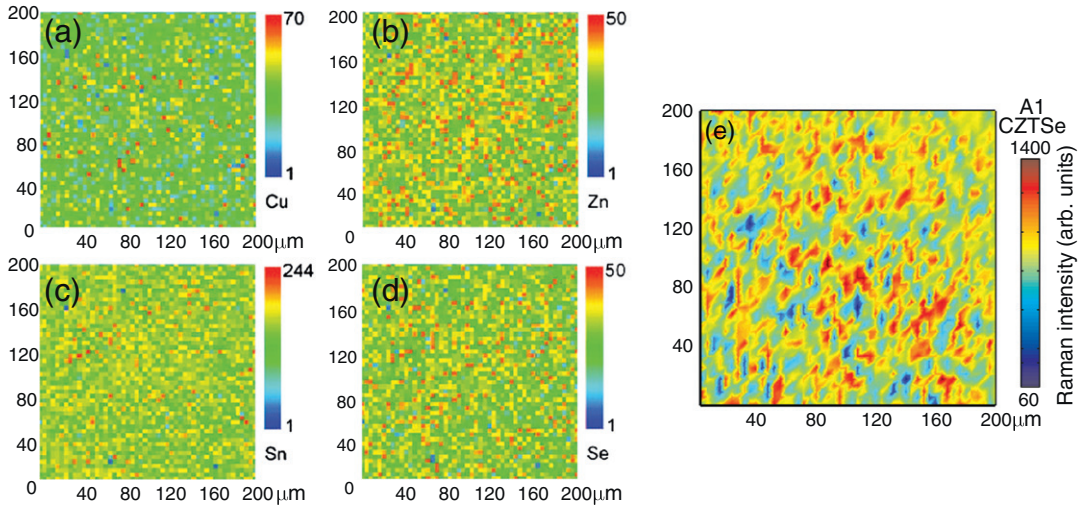

Fig. 5. Micro-PIXE intensity images of (a) Cu, (b) Zn, (c) Sn, and (d) Se concentrations of sample A. (e) Micro-Raman image for the CZTSe A_1 mode intensity of the same sample.

in the micro-PIXE images correlate with the variations in the intensity of the Raman A_1 mode.

Acknowledgments

This research was supported by the International Research & Development Program of the National Research Foundation of Korea funded by the Ministry of Science, ICT and Future Planning of Korea (Grant number: 2011-0019204) and by the New & Renewable Energy of the Korea Institute of Energy Technology Evaluation and Planning grant funded by the Korea government's Ministry of Trade, Industry and Energy (No. 20123010010130).

References

[1] S. Ahn, S. Jung, J. Gwak, A. Cho, K. Shin, K. Yoon, D. Park, H. Cheong, J.H. Yun, Determination of band gap energy (E_g) of $Cu_2ZnSnSe_4$ thin films: on the discrepancies of reported band gap values, Appl. Phys. Lett. 97 (2010) 021905.
[2] D. Park, D. Nam, S. Jung, S. An, J. Gwak, K. Yoon, J.H. Yun, H. Cheong, Optical characterization of $Cu_2ZnSnSe_4$ grown by thermal co-evaporation, Thin Solid Films 519 (2011) 7386.
[3] S. Schorr, The crystal structure of kesterite type compounds: a neutron and X-ray diffraction study, Sol. Energy Mater. Sol. Cells 95 (2011) 1482.
[4] S. Chen, X.G. Gong, A. Walsh, S.-H. Wei, Crystal and electronic and structure of Cu_2ZnSnX_4 (X = S and Se) photovoltaic absorbers: first-principles insights, Appl. Phys. Lett. 94 (2009) 041903.
[5] C. Persson, Electronic and optical properties of Cu_2ZnSnS_4 and $Cu_2ZnSnSe_4$, J. Appl. Phys. 107 (2010) 053710.
[6] M. Buffière, G. Brammertz, N. Lenaers, Y. Ren, C. Koeble, A.E. Zaghi, J. Vleugels, M. Meuris, J. Poortmans, Recombination stability in polycrystalline $Cu_2ZnSnSe_4$ thin films, Poster Presented at 39th IEEE Photovolt. Spec. Conf, 2013;
G. Brammertz, M. Buffière, Y. Mevel, Y. Ren, a.E. Zaghi, N. Lenaers, Y. Mols, C. Koeble, J. Vleugels, M. Meuris, J. Poortmans, Correlation between physical, electrical, and optical properties of $Cu_2ZnSnSe_4$ based solar cells, Appl. Phys. Lett. 102 (2013) 013902.
[7] H. Katagiri, K. Jimbo, W.S. Maw, K. Oishi, M. Yamazaki, H. Araki, A. Takeuchi, Development of CZTS-based thin film solar cells, Thin Solid Films 517 (2009) 2455.
[8] T.K. Todorov, K.B. Reuter, D.B. Mitzi, High-efficiency solar cell with earth-abundant liquid-processes absorber, Adv. Mater. 22 (2010) E156.
[9] I. Repins, C. Beall, N. Vora, C. DeHart, D. Kuciauskas, P. Dippo, B. To, J. Mann, W.-C. Hsu, A. Goodrich, R. Noufi, Co-evaporated $Cu_2ZnSnSe_4$ films and devices, Sol. Energy Mater. Sol. Cells 101 (2012) 154.
[10] S. Chen, L.-W. Wang, A. Walsh, X.G. Gong, S.-H. Wei, Abundance of $Cu_{Zn} + Sn_{Zn}$ and $2Cu_{Zn} + Sn_{Zn}$ defect clusters in kesterite solar cells, Appl. Phys. Lett. 101 (2012) 223901.
[11] S. Chen, A. Walsh, X.-G. Gong, S.-H. Wei, Classification of lattice defects in the kesterite Cu_2ZnSnS_4 and $Cu_2ZnSnSe_4$ earth-abundant solar cell absorbers, Adv. Mater. 25 (2013) 1522.
[12] S. Siebentritt, Why are kesterite solar cells not 20% efficient? Thin Solid Films 535 (2013) 1.
[13] M. Mousel, A. Redinger, R. Djemour, M. Arasimowicz, N. Valle, P. Dale, S. Siebentritt, HCl and Br_2–MeOH etching of $Cu_2ZnSnSe_4$ polycrystalline absorbers, Thin Solid Films 535 (2013) 83.
[14] R. Dargel, F. Heinemeyer, M. Köntges, J. Vogt, C. Vogt, Detection of trace impurities in Cu(In, Ga)Se2 thin film solar cells by laser ablation ICP-MS, Microchim. Acta 165 (2009) 265.
[15] M.J. Bailey, K.J. Kirkby, C. Jeynes, Trace element profiling of gunshot residues by PIXE and SEM-EDS: a feasibility study, X-Ray Spectrom. 38 (2009) 190.
[16] A. Redinger, S. Siebentritt, Coevaporation of $Cu_2ZnSnSe_4$ thin films, Appl. Phys. Lett. 97 (2010) 092111.
[17] A. Jeong, Physical properties of Cu(In,Ga)Se_2 and $Cu_2ZnSnSe_4$ thin-films grown by co-evaporation for photovoltaic applications, (Ph.D. Thesis) Department of Physics, Ewha Womans University, Republic of Korea, 2012.
[18] C.G. Ryan, PIXE and the nuclear microprobe: tools for quantitative imaging of complex natural materials, Nucl. Instrum. Methods Phys. Res. Sect. B 269 (2011) 2151.
[19] G. Suresh Babu, Y.B. Kishore Kumar, P. Uday Bhaskar, V. Sundara Raja, Effect of Cu/(Zn + Sn) ratio on the properties of co-evaporated $Cu_2ZnSnSe_4$ thin films, Sol. Energy Mater. Sol. Cells 94 (2010) 221.
[20] A. Nagaoka, K. Yoshino, H. Taniguchi, T. Taniyama, H. Miyake, Growth of $Cu_2ZnSnSe_4$ single crystals from Sn solutions, J. Cryst. Growth 354 (2012) 147.
[21] M. Altosaar, J. Raudoja, K. Timmo, M. Danilson, M. Grossberg, J. Krustok, E. Mellikov, $Cu_2Zn_{1-x}Cd_xSn(Se_{1-y}S_y)_4$ solid solutions as absorber materials for solar cells, Phys. Status Solidi A 205 (2008) 167.
[22] M. Grossberg, J. Krustok, K. Timmo, M. Altosaar, Radiative recombination in $Cu_2ZnSnSe_4$ monograins studied by photoluminescence spectroscopy, Thin Solid Films 517 (2009) 2489.
[23] G. Marcano, C. Rincón, L.M. de Chalbaud, D.B. Bracho, G.S. Pérez, Crystal growth and structure, electrical, and optical characterization of the semiconductor Cu_2SnSe_3, J. Appl. Phys. 90 (2001) 1847.
[24] A.S. Opanasyuk, D.I. Kurbatov, M.M. Ivashchenko, I.Yu. Protsenko, H. Cheong, Properties of the window layers for the CZTSe and CZTS based solar cells, J. Nano- Electron. Phys. 4 (2012) 01024.
[25] J.F. Scott, T.C. Damen, W.T. Silfvast, R.C.C. Leite, L.E. Cheesman, Resonant Raman scattering in ZnS and ZnSe with the cadmium laser, Opt. Commun. 1 (1970) 397.
[26] X. Fontané, L. Calvo-Barrio, V. Izquierdo-Roca, E. Saucedo, A. Pérez-Rodriguez, J.R. Morante, D.M. Berg, P.J. Dale, S. Siebentritt, In-depth resolved Raman scattering analysis for the identification of secondary phase: characterization of Cu_2ZnSnS_4 layers for solar cell applications, Appl. Phys. Lett. 98 (2011) 181905.
[27] A. Redinger, K. Hönes, X. Fontané, V. Izquierdo-Roca, E. Saucedo, N. Valle, A. Pérez-Rodríguez, S. Siebentritt, Detection of a ZnSe secondary phase in coevaporated $Cu_2ZnSnSe_4$ thin films, Appl. Phys. Lett. 98 (2011) 101907.

Please cite this article as: D. Nam, et al., Composition variations in $Cu_2ZnSnSe_4$ thin films analyzed by X-ray diffraction, energy dispersive X-ray spectroscopy, particle induced ..., Thin Solid Films (2014), http://dx.doi.org/10.1016/j.tsf.2014.03.079